Pak.j.stat.oper.res. Vol.22 No.2 2026 pp 177-189 DOI: http://dx.doi.org/10.18187/pjsor.v22i2.5130

Pakistan Journal of Statistics and Operation Research

Atypical Functional Brain Regions Identification in Children with Autism Spectrum Disorder Using One-Class SVM and fMRI-Derived Graph-Theoretic Parameters

Muhammad Farooq[1*], Muhammad Kashif Saleem[2], Tahir Abbas[3]

*Corresponding author

1. Department of Statistics, College of Science, Sultan Qaboos University, Muscat, Oman, m.farooq@squ.edu.om
2. Department of Statistics, Government College University Lahore, Pakistan, ranakashifpu@gmail.com
3.Department of Mathematics, College of Science, University of Sharjah,Sharjah, United Arab Emirates, tabbas@sharjah.ac.ae

Abstract

Autism spectrum disorder (ASD) is a complex neurodevelopmental condition that typically emerges in early childhood and persists throughout life, making early and objective detection crucial. This study integrates graph theoretic approach with anomaly detection approaches to identify atypical functional brain regions in children aged up to 5 years with ASD. Resting-state fMRI data of 53 ASD and 53 healthy subjects were used to construct functional connectivity matrices were across 32 functional regions of interest, from which graph theoretic features were extracted. The one-class SVM achieved an AUC of 0.733 in identifying atypical regions. Atypicality was observed in the salience network , specifically, in the supramarginal gyrus, anterior cingulate cortex and left anterior insula. In the visual network, medial occipital and laterl occipital regions were identified as atypical. The language network showed atypical regions in the right inferior frontal gyrus and the left posterior superior temporal gyrus. The dorsal attention network exhibited atypicality in the right frontal eye field region. Graph-theoretic analysis to regional atypicality highlighted disruptions in integration, segregation, and hub-related characteristics.

Key Words: Autism Spectrum Disorder; Graph-Theoretic Measures; One-Class Support Vector Machines; rs-fMRI, sMRI

Mathematical Subject Classification:

1. Introduction

The brain is one of the most imperative organs of the human body. Human's brain functioning can be compromised by genetic factors and lifestyle choices, often culminating in diseases like parkinson, depression and autism spectrum disorder (ASD). Medication proves effective in curing several diseases like depression and anxiety, but for conditions like ASD, a cure remains elusive (Millan et al., 2015). The primary causes of ASD are environmental and genetic (Hallmayer et al., 2011). The intensity of symptoms fluctuates significantly among individuals, however, the onset of certain ASD symptoms commonly occurs at the age of two years (Ecker et al., 2015). According to the World Health Organization, ASD is prevalent in 1 of 100 children (Zeidan et al., 2022) where boys are four times more likely to be autistic than girls. Moreover, the Global Burden of Disease Study report revealed that ASD has affected 28 million people and contributed to 4.31 million disability-adjusted life years (Li et al., 2022).

Neuroimaging is a noninvasive brain image approach to investigate brain structure and function. Resting-state func-

tional magnetic resonance imaging (rs-fMRI) is the most powerful approach to study intrinsic brain activity by measuring blood oxygen level dependent (BOLD) changes over time across regions of interest, when the subject under observation is not allowed to respond to stimuli or perform any task (Canario et al., 2021). Graph theory provides tools for in-depth examination of functional connectivity by constructing nondirectional graphs for each subject. These graphs analyze the topological features of functional connectivity across ROIs, see Bullmore and Sporns (2009), Zamani et al. (2022), Ebadi et al. (2017), Iswarya et al. (2019) for more details. These graph theoretic measures from rs-fMRI are powerful biomakers and have been used in several studies to classify ASD using machine learning techniques, for example, support vector machines(Shi et al. (2020)),Mutli-scale graph convolutional network (Chu et al. (2022)), multi-label graph concolutional network (Vankara et al. (2024)) and references therein.

Beyond classifying ASD, identification of anomalous brain regions is an equally important goal. These anomalous regions are generally characterized by altered functional integration, disrupted information flow or abnormal topological properties within brain network. The regional abnormalities often correspond to deficit in social cognition, communication, sensory processing and motor control. Consequenty, many studies have focused on localizing ASD-related anomalies using statistical and machine learning based analysis of brain connectivity graphs. Studies have mostly used group level statistical analysis such as t-tests, ANOVA, permutation testing and non-parametric comparison to identify atypical brain regions (Sadeghi et al. (2017); Pourmotahari et al. (2024),Kazeminejad and Sotero (2019)), however inability of capturing individual-specific, dynamic and hetrogeneous brain alteration limits their effectiveness in identifying true brain regions. Another approached considered in literature to determine anomalous ASD brain regions is the use of unsupervised machine learning approaches. For example, geometry-inspired graph Ricci curvatures (Elumalai et al. (2022)), Hidden Markov Model (HMM) combined with dynamic graph theory to characterize time-varying connectivity states (Qian et al. (2024)), unsupervised manifold learning on high-order morphological brain networks (Soussia and Rekik (2018)). More recent approaches, such as unsupervised graph neural networks (GNNs) and hypergraph-based anomaly detection ((Wang and Ding, 2025), Sadeghian et al. (2025)), have modeled higher-order interactions and learned node embedding to identify atypical activity.

In the present study, we propose a graph-based anomaly detection framework using one-class SVMs(OC-SVM). The OC-SVM is an unsupervised learning algorith that learns the boundry from normal subjects data distribution and identifies subjects that deviates from it as anomalies. Previous studies have demonstrated the effectiveness of OC-SVM and OCC-inspired approaches for identifying atypical brain patterns in ASD across multiple imaging modalities. For example,Retico et al. (2016) applied OC-SVM to sMRI derived morphometric features and identified abnormalities in language related areas and defalut mode network. In contrast to previous studies that employed whole-brain morphometric or large-scale multimodal connectivity features, our work focuses on a more localized and functionally coherent parcellation comprising 32 functional regions. In addition, we consider node-level graph-theoretic measures; degree, clustering coefficient, local efficiency, global efficiency, average pathh length and betweenness centrality as features to implement OC-SVM alongside other anomaly detection methods. After selecting best anomaly detection approach based on performance metrics, we then identify region-specific functional anomalies at the individual level. This design enables a more fine-grained characterization of atypical network organization, emphasizing regional deviations in connectivity topology rather than global or population-level differences.

The rest of the article is organized as follows: Section 2 describes the material and methods, including data preprocessing, graph-theoretic feature extractions, and anomaly detection approaches. Section 3 presents results, focusing on the selection of best anomaly detection method based on performance metrics, the identification of atypical brain regions and thier spatial mapping, and an analysis of the contribution of graph-theoretic parameters to regional brain atypicality. Finally, Section 4 provides the conclusion with recommendations for future research.

2. MATERIALS AND METHODS

2.1. Data

In this study, we utilized rs-fMRI and sMRI scans from the publicly accessible Autism Brain Imaging Data Exchange, ABIDE I repository, contributed by twenty-four international brain imaging laboratories with a collection of scans of 1112 (539 ASD, 573 control) subjects. Detailed information on image acquisition and corresponding parameters is available in (Di Martino and Mostofsky, 2023). We restricted our analysis to participants aged 5 to 10 years. This age restriction was applied to focus on identifying ASD subjects during early developmental stages. This reduces the subject to 116 (ASD 54 and control 62) a in ABIDE I subjects from which we have selected 53 ASD and 53 healthy to make equal representation. The purpose of the sMRI scans were used during preprocessing to improve anatomical

registration, tissue segmentation, normalization to MNI space, and accurate ROI extraction.

2.2. Preprocessing and Denoising

Preprocessing of the rs-fMRI and sMRI data was performed to remove artifacts and standardize the images for subsequent analyses. The CONN toolbox in MATLAB v2021 (Nieto-Castanon and Whitfield-Gabrieli (2021)) was used for both preprocessing and graph-theory analysis. We employed CONN's default MNI preprocessing pipeline, which includes functional realignment, slice-timing correction, structural segmentation and normalization, functional normalization, outlier detection, and spatial smoothing. Functional images were realigned to a mean BOLD image, and each subject's T1-weighted sMRI scan was used to guide functional–structural coregistration, tissue segmentation, and spatial normalization using the unified segmentation framework in SPM12 (Ashburner and Friston (2005)). Both structural and functional data were normalized to MNI space and resampled to 1-mm and 2-mm isotropic voxel sizes, respectively. Outlier volumes were identified using motion and global BOLD signal change criteria, and these flagged scans were included later as nuisance regressors during denoising. Functional smoothing was performed using an 8-mm full-width at half-maximum (FWHM) Gaussian kernel to increase the signal-to-noise ratio (smoothing was applied only to functional data, not anatomical scans). Despite preprocessing, non-neural signal fluctuations related to motion, outlier volumes, and physiological noise remained in the BOLD signal; therefore, CONN's default denoising pipeline was applied. This included regression of white-matter and cerebrospinal-fluid components (CompCor), realignment parameters, identified outlier scans, and linear trends, followed by temporal band-pass filtering (0.008–0.09 Hz). The effectiveness of denoising was evaluated by examining the distribution of functional connectivity values before and after denoising. Before denoising, the distribution was positively skewed with high inter-subject and inter-session variability, whereas after denoising it became approximately centered with reduced variability (see, Figure 1), indicating improved stability of the BOLD signal and enabling more reliable extraction of functional connectivity measures.

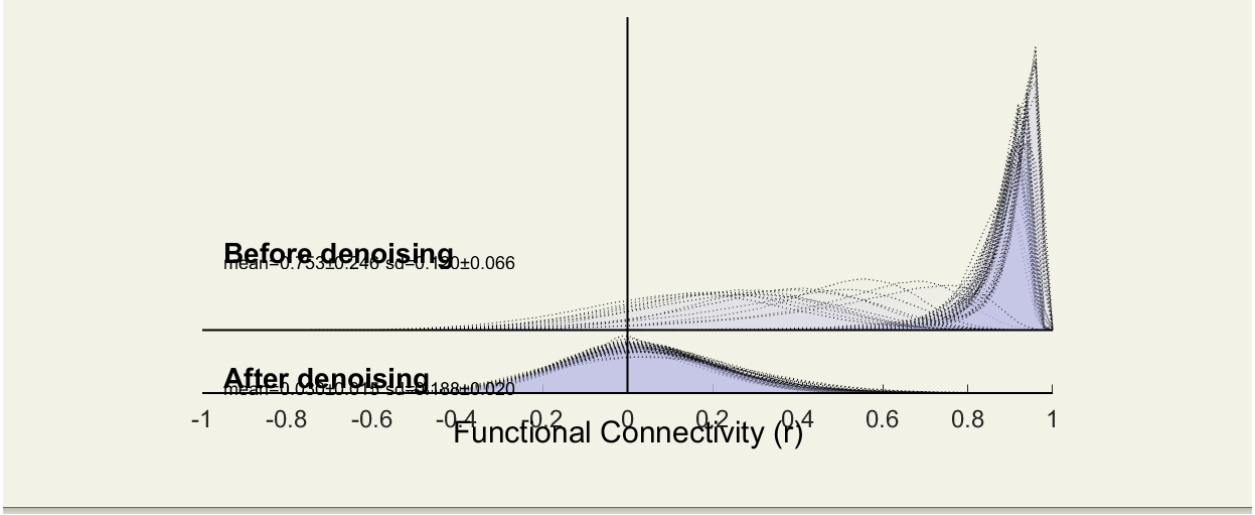

Figure 1: Distribution of functional connectivity (FC) values before (top) and after (bottom) denoising.

The mean correlation coefficients before denoising was 0.7531 which shifted to 0.036 after denoising. Similarly, the we see a moderate reduction in standard deviation from 0.19 ± 0.066 (before denoising) to 0.188 ± 0.020 after denoising. This shift indicates reduced inter-subject and inter-sessional variability, allowing for the extraction of smoother BOLD signals from the scans.

2.3. Functional Connectivity and Graph-Theoretic Feature Extraction

During an fMRI scan, the neural activity within a specified brain region is summarized by ROI time series. This time series was generated by averaging the BOLD signal across all voxels within an ROI at acquisition time point. In this study, ROIs were defined as 32 network nodes derived from Yet at al 7-network functional parcellation, including bilateral cortical hub and cerebellar extensions, represented as spherical ROIs in MNI space. The Yet al al. 7-network parecllation was selected as it provides functionally meaningful representation of large scale ROI that aligned with

the study objectives. Additionally, this parcellation facilities consistency with graph-theoretic measures derived from functional connectivity analysis.

Functional connectivity between ROIs of brain was characterized by correlation matrix derived from each subject ROIs time series data. Each element $r_{i,j}$ of the matrix represents Pearson correlation coefficient between time series t_i and t_j of i-th and j-th ROIs. This ROI-to ROI correlation (RRC) matrix is generally refereed as functional connectivity matrix, and was generated in CONN after applying the following Fisher transformation

$$z_{i,j} = \frac{1}{2} ln \left(\frac{1 + r_{i,j}}{1 - r_{i,j}} \right) \tag{1}$$

The transformed $z_{i,j}$ values are approximately Gaussian distributed which support the subsequent analysis.

The connectivity patterns derived from RRC matrix across brain regions are highly complex. Graph theory provides a powerful framework to quantify and interpret these patterns by characterizing topological properties of brain connectivity networks. Prior to computing graph-theoretic metrics, the diagonals and negative correlations were replaced with zero. The RCC matrices were threshold using the proportional thresholding approach to retain the strongest connections. A network density range of 10-20% was examined, and a threshold $z > 0.22$ was selected based on area under curve (AUC) analysis. Subsequently, graph measures were computed using the CONN toolbox.

These metrics fall into three categories: functional integration, functional segregation and local nodal centrality. Functional integration measures the global communication efficiency across the entire network. Two well-known indicators of functional integration are average path length and global efficiency. The average path length is defined as the average shortest distance between all pairs of nodes. Global efficiency is a complementary measure that computes the average of the inverse shortest path lengths across the network. The functional segregation refers to the tendency of forming densely interconnected clusters of brain regions. It is measured based on the metrics such as the clustering coefficient and local efficiency. The clustering coefficient represents the proportion of ROIs that are connected to a certain ROI and the local efficiency measures the efficiency of information transfer within a local network. Finally, the local nodal centrality quantifies the importance of ROI within the brain network using measures such as degree and betweenness centrality. Degree is defined as the total number of edges connected to a specific node or ROI. From a neurobiological standpoint, a region of high degree is interpreted as having extensive functional and anatomical interactions with many other regions in a brain network (Ebadi et al. (2017)). Betweenness centrality quantifies the proportion of shortest paths between all pairs of nodes in the network that traverse a particular node (Brentani et al. (2013), Freeman et al. (1979)).

2.4. Statistical and Machine Learning Approaches for Anomaly Detection

Three approaches have been considered, namely, robust Mahalanobis distance, auto-encoder and one-class support vector machines.

2.4.1. Robust Mahalanobis Distance

The Mahalanobis distance (MD) is a multivariate metric used to measures the distance of an observed vector $x \in \mathbb{R}^p$ from the mean of a distribution $\mu \in \mathbb{R}^p$ accounting for the covariance matrix $\Sigma \in \mathbb{R}^{p \times p}$, that is

$$D_M(x) := \sqrt{(x - \mu)^T \Sigma^{-1} (x - \mu)} \tag{2}$$

If $x \sim N(\mu, \Sigma)$ a multivariate normal distribution, then $D_M^2(x) \sim \chi_p^2$, and a point x is flagged as an anomaly if $D_M^2(x) > \chi_{p,1-\alpha}^2$, a $(1-\alpha)$-quantile of the chi-square distribution with p degree of freedom. Note that the MD-type distances assume that the data have well-defined mean and covariance. In addition, it assume that the covariance matrix is invertible. In high dimensional or ill conditioning dataset (n¡p), Σ can be unstable. The Ledoit–Wolf estimator improves the conditioning of covariance matrix by shrinking it towards the well-behaved target matrix. Fomally, the Ledoit–Wolf covariance matrix is defined by

$$\Sigma_{LW} := (1 - \lambda) S + \lambda T \tag{3}$$

where S is the sample covariance matrix, T is the target matrix and $\lambda \in [0,1]$ is the shrinkage parameter determined externally. Consequently, the robust Mahalanobis distance (RMD) is defined by

$$D_{RMD}(x) := \sqrt{(x-\mu)^T \Sigma_{LW}^{-1}(x-\mu)} \tag{4}$$

A point $x \in \mathbb{R}^p$ is called anomalous if $D^2_{RMD}(x) > \chi^2_{p,1-\alpha}$

2.4.2. Autoencoder-Based Anomaly Detection Model

Autoencoders (AE) are unsupervised machine learning algorithms that learns compact, low dimensional representation of input data through a self-reconstruction objective. It comprises of two components; an encoder and a decoder. The encoder maps the high dimensional input $x \in \mathbb{R}^p$ into a compressed latent low dimensional representation $z \in \mathbb{R}^k$ $(k \ll p)$ using a series of nonlinear transformation:

$$z := f_\theta(x) = \sigma(W_e x + b_e)$$

while the decoder reconstruct the input from this latent code, that is

$$\hat{x} := g_\phi(z) = \sigma(W_d z + b_d)$$

where W_e, W_d denote weight matrices, b_e, b_d are biases and $\sigma(\cdot)$ is the activation function. The network is trained to minimize the reconstruction loss, most commonly, squared loss between the original the original input and its reconstruction. For a single input $x \in \mathbb{R}^p$, the reconstruction loss is defined as:

$$\mathcal{L}_{\text{rec}}(x, \hat{x}) \frac{1}{p} \sum_{j=1}^{p} (x_j - \hat{x}_j)^2 . \tag{5}$$

Given data set $\{x^{(i)}\}_{i=1}^N$, the training objective is formulated as:

$$\min_{\theta,\phi} \frac{1}{N} \sum_{i=1}^{N} \mathcal{L}_{\text{rec}} \left(x^{(i)}, \hat{x}^{(i)} \right) + \lambda \sum \|W_l\|_2^2 , \tag{6}$$

where λ is the regularization parameter that controls model complexity and mitigates overfitting.

2.4.3. One-Class Support Vector Machines

The One-Class Support Vector Machines (OCSVM) is an unsupervised learning algorithms primarily used for anomaly detection and outlier identification. Unlike binary SVMs which is trained on labeled data of two classes, OCSVM is trained on data from a single class and construct an hyperplane that separates the target set from origin with maximal margin. For more complex data, an implicit mapping of data into higher dimensional space (feature space) is defined such that dot product into the feature space can be evaluated by kernel function. The optimization problem can be formulated as:

$$\begin{aligned} \min_{w,\xi_i,\rho} \quad & \frac{1}{2}\|w\|^2 + \frac{1}{\nu n} \sum_{i=1}^{n} \xi_i - \rho \\ \text{subject to} \quad & (w \cdot \phi(x_i) \geq \rho - \xi_i, \\ & \xi_i \geq 0, \quad i = 1, \ldots, n \end{aligned} \tag{7}$$

where $\nu \in (0,1]$ is the regularization parameter. A test sample is classified as inlier or outlier depending on whether it lies within or outside the learned decision boundary. Different kernel functions such as the sigmoid, polynomial and radial basis function (RBF) are commonly uesd to evaluate inner product in feature space. Among these, RBF kernel is often preferred due to its ability to capture non-linear relationship effectively and defined as:

$$K(x_i, x_j) = \exp\left(-\gamma \|x_i - x_j\|^2\right) \tag{8}$$

where $\gamma > 0$ is a kernel parameter that determines the width of the Gaussian function.

2.4.4. Performance Evaluation Metrics

After implementing anomaly algorithms, subject level analysis was performed to identify the subject anomalous (ASD) or normal (control). Several evaluation metrics were then employed to compare the performance of anomaly detection ability of algorithms by comparing prediction with true labels. Following is the brief description:

Sensitivity measures the proportion of true positive correctly identified by algorithm

$$\text{Sensitivity} = \frac{TP}{TP + FN}$$

where TP and FN denote the number of true positives and false negatives, respectively. Higher sensitivity indicates better detection ability of the algorithm.

Specificity measures the proportion of true negative correctly identified by algorithm

$$\text{Specificity} = \frac{TN}{TN + FP}$$

where TN and FP denote the number of true negative and false positive, respectively. Higher value indicates better algorithm's performance.

Precision measures the proportion of correclty predicted positive cases among all predicted positive cases

$$\text{Precision} = \frac{TP}{TP + FP}$$

F_1 **Score** is the harmonic mean of precision and sensitivity which provide a balance trade-off between false positive and false negative

$$F1 = 2 \times \frac{\text{Precision} \times \text{Sensitivity}}{\text{Precision} + \text{Sensitivity}} \tag{9}$$

Area Under the Receiver Operating Characteristic Curve (AUC) and Permutation Testing quantifies the algorithm's overall ability to discriminate between two classes. The higher AUC indicates better performance of the algorithm. To further evaluate the statistical significance of observed AUC, permutation testing was conducted. In this approach, class labels were randomly shuffled multiple times to generate a null distribution of AUC under the assumption of no true class separation. The permuation based p-value was calculated to determined whether the observed performance was significantly greater than the by chance expected performance.

3. Results and Discussion

3.1. Experimental Setting

Prior employing anomaly detection algorithms, data was reshaped into long-format representation. where each observation corresponded to specific subject-ROI pair. Consequently each subject contributed 32 observations, one per ROI, described by six graph parameters. This resulted in total 3392 samples (106×32), with each 6 features. To prevent information leakage, only control subjects were used for training, validation and testing. The reshaped data for the control subjects were randomly divided into training $(60\% = 992)$, validation $(20\% = 352)$, and test $(20\% = 352)$, ensuring that all ROIs of one subject were assigned exclusively to one data split. Feature standardization scaling was applied estimating parameters mean and variance from training split to prevent information leakage, and extended this transformation to the validation and the test parts.

Hyperparameter optimization of the autoencoder was achieved using a structured grid search over architectural and training parameters. It included encoder and decoder capacity, bottleneck dimensionality, regularization, learning rate and batch size. The search evaluated hidden layer size of 8 to 64 neurons, latent dimensions of 1 to 4 and network depth of 1 or 2 layers. Furthermore, regularization is controlled by L_2 weight decay (0 to 1×10^{-3}), drop out rates (0 -0.2), learning rate 3×10^{-4} to 3×10^{-3} and batch size of 16 to 64. Similarly, for OCSVM, hyperparamter tuning was conducted using a grid search over $\nu \in \{0.01, 0.03, 0.05, 0.08, 0.10, 0.15\}$ and $\gamma \in \{0.1, 0.3, 0.5, 0.7, 1.0, 2.0, 3.0\}$. The hyperparameters tunning in both algorithms was performed using subject-level 5-fold cross validation on control subjects only.The model training and statistical analysis was performed using Python-based scientific computing tools.

3.2. Performance Comparison of Anomaly Detection Algorithms

Among the three methods, OCSVM performed better based on all performance measures at subject level. It achieved highest mean ROC AUC (0.726+-0.112), indicating strong global discrimination between ASD and control subjects. The robustness of observed separation is further supported by the significance of permutation test (p-value=0.00099). The sensitivity, specificity, F_1 scores and precision are 0.735, 0.644, 0.668 and 0.697, respectively. In the case of AE, the mean ROC AUC is 0.653 ± 0.082 with statistical significance performance under permutation testing (p-value=0.00699), however, it showed low sensitivity (0.531) indicating low ability to detect ASD cases. In contrast, RMD showed limited discriminating power with ROC AUC (0.563 ± 0.171) and non-significant permutation results (p-value = 0.0629). The other performance measures also achieved low values for RMD as shown in Table 1.

Metric	Autoencoder	One-Class SVM	Robust Mahalanobis
ROC AUC	0.653 ± 0.082	$\mathbf{0.726 \pm 0.112}$	0.563 ± 0.171
Sensitivity	0.531 ± 0.164	$\mathbf{0.735 \pm 0.155}$	0.593 ± 0.270
Specificity	$\mathbf{0.716 \pm 0.129}$	0.644 ± 0.095	0.447 ± 0.277
Precision	0.665 ± 0.065	$\mathbf{0.668 \pm 0.100}$	0.539 ± 0.105
F1-Score	0.572 ± 0.105	$\mathbf{0.697 \pm 0.120}$	0.525 ± 0.166
Permutation p (AUC)	0.006993	**0.000999**	0.062937

Table 1: Subject-level performance comparison of anomaly detection methods. Models were trained using control subjects only and evaluated for discriminating ASD from control subjects. Values are reported as mean ± standard deviation.

These findings suggests that the kernel-based algorithm can effectively separate atypical functional connectivity patterns in ASD from control even for small and moderate dimensional fMRI data. Comparable AUC values (0.75-0.79) have been reported in previous studies (Wang et al. (2023); Sewani and Kashef (2020)) where large data set was considered with autoencoder or semi-supervised deep learning approaches.This shows that OCSVM results are consistent with prior studies despite the samll sample used in this study.

3.3. Identification and Spatial Mapping of Atypical ASD Brain ROIs

To identify atypical brain regions associated with ASD, we considered OCSVM in the following because of its superior performance related to alternative anomaly detection approaches. Two criteria; Cohen's d and odds ratio, were applied to determine atypical ROIs. Cohen's d measures the effect size to assess the magnitude of group-level differences between ASD and control participants while odds ratio measures the prevalence of anomalies in the ASD group compared to controls. We considered Cohen's $d > 0.40$ and Odds ratio > 1 which resulted eight anomalous ROIs. The medium level of Cohen's d threshold was selected to identify brain regions exhibiting meaningful group differences due to inter-subject variability, measurement noise and small sample size, see for example, Poldrack (2007). The additional criteria odds ratio > 1 ensures that the selected regions are positively associated with ASD, reflecting increased likelihood of abnormality. The results presented in Table 2 show that the identified ROIs spanned four major functional networks: the salience network, visual network, language network, and dorsal attention network.

The Salience network emerged as the most affected system, with regions: right supramarginal gyrus (SMG), anterior cingulate cortex (ACC), and left anterior insula. These regions showed moderate-to-large effect sizes (Cohen's: 0.40 - 0.58) and high odds ratios, indicating both substantial group differences and high prevalence of anomalies in individuals with ASD. These finding align with prior work identifying SN dysfunction dysfunction as central to social and emotional deficits (Attanasio et al. (2024); Toyomaki and Murohashi (2013)). Moreover, evidences (Odriozola et al. (2016); Yang et al. (2018); Francis et al. (2019)) implicates that the ACC and aterior insula in disrupted integration of interoceptive and social-emotional signals, while the SMG has been linked to atypical social cognition and attentional reorienting in ASD.

The visual network abnormalities were observed in both medial and lateral occipital regions. The effect sizes of these regions ranging from 0.54 to 0.57 with odds ratio ranging from 1.97 to 2.70, indicating moderate group level differences and moderate increases in anomaly prevalence. The prior studies have consistently demonstrated disrupted instrinsic connectivity within the visual network,particularly, involving the occipital pole adn middle occipital gyrus (Bi et al. (2018); Xu et al. (2019)). Additionally, Nickl-Jockschat et al. (2012) reported gray matters abnormalities across medical and lateral occipital cortices. Task-based fMRI studies further indicate atypical occipital activation pattern during visual stimulation in ASD (Aoki et al. (2019)). Collectively, these findings reinforce that atypical connectivity and structure in medial and lateral occipital regions underlie the visual perceptual and integration abnormalities

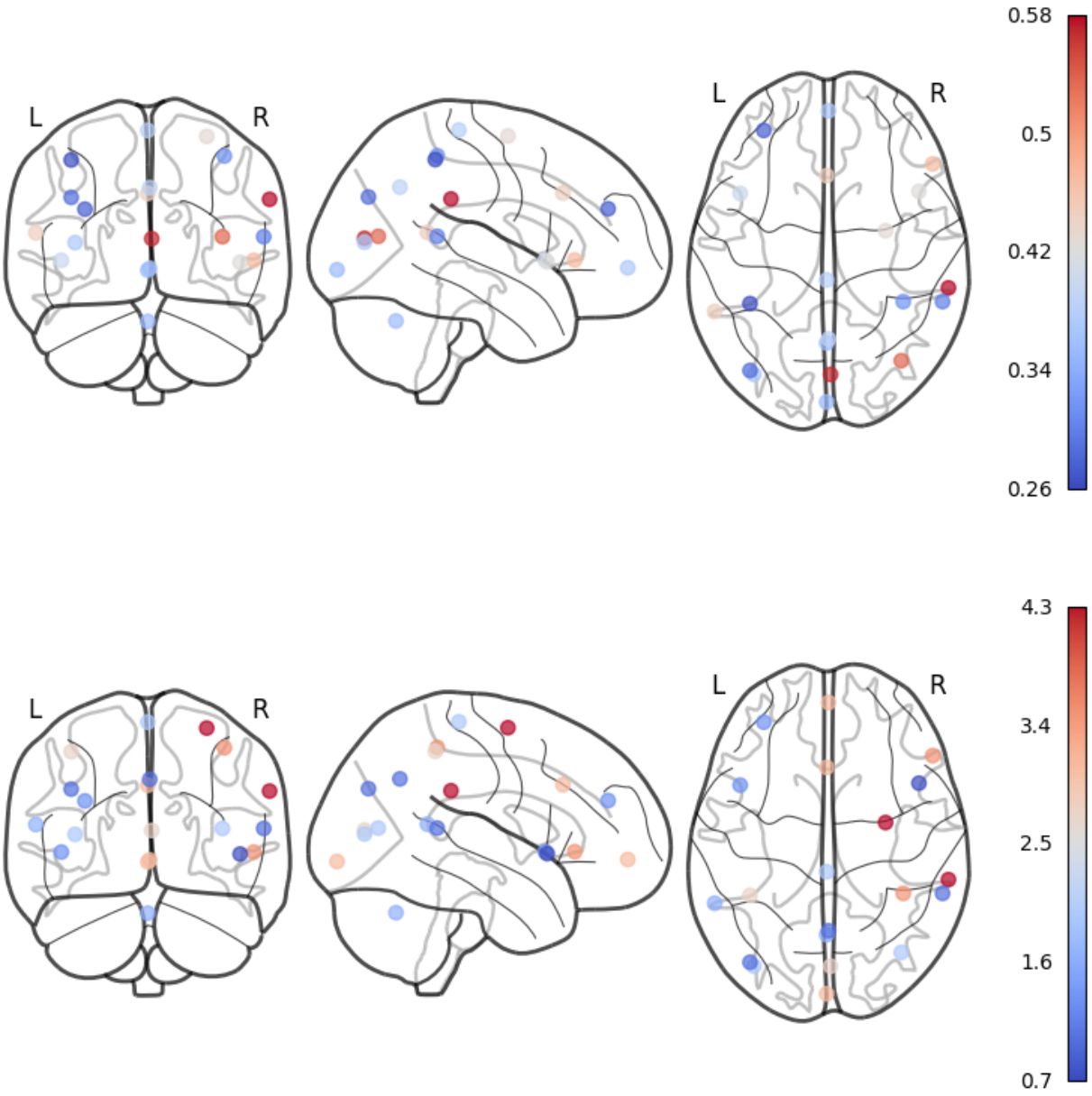

Figure 2: Whole-brain mapping of regional effects derived from the OC-SVM analysis. The upper panel shows the spatial distribution of regions colored according to the signed Cohen's d values (ASD vs control), reflecting the magnitude and direction of group differences. The lower panel depicts the corresponding regional distribution based on the odds ratio (ASD vs. control), indicating relative enrichment of anomalous patterns across brain regions.

Network	Region	Cohen's d	Odds Ratio
Salience	SMG (R) (62;-35;32)	0.580	4.346
Visual	Medial (2;-79;12)	0.569	2.695
Visual	Lateral (R) (38;-72;13)	0.537	1.974
Language	IFG (R) (54;28;1)	0.469	3.483
Language	pSTG (L) (-57;-47;15)	0.446	1.636
Salience	ACC (0;22;35)	0.444	3.080
Dorsal Attention	FEF (R) (30;-6;64)	0.428	4.346
Salience	AInsula (L) (-44;13;1)	0.400	1.312

Table 2: Anomalous brain regions exhibiting moderate-to-large effect sizes (Cohen's $d > 0.4$) and increased odds of anomalous expression in the ASD group compared to controls (Odds Ratio > 1.0). Regions are grouped by functional network

characteristics of ASD.

The language network also demonstrated notable atypicality, particularly in the right inferior frontal gyrus (IFG) and left posterior superior temporal gyrus (pSTG). The effect size is slightly low ranging from 0.45 to 0.47 but the right IFG showed a comparatively high odds ratio (3.48), indicating a substantial portion of ASD individuals exhibiting anomalies in this region. Consistent results are reported by Lee et al. (2017) suggesting weekened frontotemporal integration within the language networks. Similarly, Duan et al. (2022) identified structural abnormalities in the right IFG and bilateral STG linking them communication impairments.

Finally, the right frontal eye fiedl (FEF) region in the dorsal attention network demonstrated a moderate effect size (Chohen d = 0.43) and one of the highest odds ratios (4.35). This finding suggests that attentional control and goal-orienting mechanisms are frequently atypical in ASD. A similar abnormal dynamic coupling of the right FEF with frontoparietal areas was reported by Ma et al. (2022). The high odds ratio associated with the FEF highlights its potential relevance as a biomarker of attentional dysregulation within ASD. The spatial visualization of the identified atypical ROIs based on Chohen's d and Odds ratios is shown in Figure 2 for further illustration.

3.4. Graph-Theoretical Measures Contribution in Atypicality of ASD ROIs

To further characterize the network-level properties underlying the identified atypical ROIs, we examined the relative contribution of graph-theoretic parameters as summarized in Table 3.

Network	Region	APL	GE	LE	CC	BC	Deg	Dominant Parameter	Max OR
Salience	ACC (0;22;35)	0.249	0.257	0.009	0.020	0.386	0.078	BC	2.695
Salience	AInsula (L) (-44;13;1)	0.309	0.199	0.025	0.019	0.177	0.271	APL	1.312
Salience	SMG (R) (62;-35;32)	0.221	0.252	0.098	0.063	0.153	0.212	GE	7.519
Visual	Lateral (R) (38;-72;13)	0.370	0.291	0.016	0.025	0.050	0.248	APL	2.327
Visual	Medial (2;-79;12)	0.272	0.225	0.107	0.115	0.092	0.189	APL	2.327
Language	pSTG (L) (-57;-47;15)	0.114	0.055	0.247	0.156	0.306	0.122	BC	2.327
Language	IFG (R) (54;28;1)	0.206	0.030	0.142	0.287	0.238	0.095	CC	2.336
Dorsal Attention	FEF (R) (30;-6;64)	0.048	0.246	0.174	0.142	0.169	0.221	GE	4.398

Table 3: ROI-level contribution summary across graph-theoretical parameters, arranged by functional network. APL: Average Path Length; GE: Global Efficiency; LE: Local Efficiency; CC: Clustering Coefficient; BC: Betweenness Centrality; Deg: Degree.

In Salience network, atypicality was primarily associated with altered integrative and hub-related properties. The betweeeness centrality showed relatively dominant contribution indicating disrupted control over information flow, where the anterior insula and supramarginal gyrus were mainly influenced by average path length and global efficiency. This indicates a reduced network integration in ASD in these regions compared to control. This is consistent with the prior work showing that core salience network nodes, particularly, anterior cingulate cortex (ACC) and anterior insula exhibits altered information flow (Itahashi et al. (2014)). Visual network regions showed relatively dominant contribution of average path length, reflecting impaired global integration. This is supported by previous graph theoretic studies reporting increased path length and reduced global efficiency in ASD (Keown et al. (2017)). The language network regions showed altered local segregation in the right inferior frontal gyrus and disrupted information transfer in the left posterior superior temporal gyrus. This findings is consistent with prior studies reports of disrupted local segregation and altered temporal-frontal connectivity underlying impairments in ASD (Harlalka et al. (2018)). Finally, the reduced

global efficiency in the right frontal eye field (FEF) within the dorsal attention network aligns with the prior evidence of atypical connectivity in attention network in ASD (Keown et al. (2017), Harlalka et al. (2018)). This support the interpretation of impaired global integration within attention-control systems in ASD.

4. CONCLUSION

The combination of rs-fMRI and sMRI during preprocessing, coupled with implementation of anomaly detection algrothims based on graph-theoretic parameters, offers a promising avenue for identification of ASD atypical ROIs. This research effectively employed a comprehensive strategy, melding ROI-to-ROI analysis, graph theory, and one-class SVM to identify atypical brain regions of ASD children aged upto 5 years. The findings highlighted atypical regions in different networks sucha as SMG, ACC and left anterior insula regions in Salience network, medial an lateral occipital regions in visual networks, right inferior gyrus and left posterior superior temporal gyrus in language network and right frontal eye field region in dorsal attention networks. In addition, the contribution of graph theoretic measure in the context of atypicality in identified regions were also investigated, indicating that network and region specific disruptions is in integration, segregation and hub-related properties.
The robustness and applicability of the proposed approach can be enhanced with several key consideration. Firstly, this study considered data from ABIDE I. One can incorporate data from several other sources to prevent biases. Moreover, incorporating information from various brain imaging projects can contribute to a more comprehensive understanding of atypicality in brain regions. Secondly, this study focused on the age group of upto 5 years. Expanding the age range of patients would also have been beneficial for a more nuanced analysis. Distinct patterns in neuroimaging data across different age groups could have been better understood, allowing for insights into age-related variations. Thirdly, it would be advantageous to consider additional imaging modalities like diffusion tensor imaging (DTI) or positron emission tomography (PET) alongside rs-fMRI and sMRI.

Acknowledgements

This research uses data from the Autism Brain Imaging Data Exchange (ABIDE) dataset, collected and shared by the ABIDE consortium (`https://fcon_1000.projects.nitrc.org/indi/abide/`). We gratefully acknowledge the contributions of the participants, researchers, and funding agencies that made this dataset possible. The ABIDE dataset is a multisite, cooperative effort aimed at providing a large-scale repository of brain imaging and phenotypic data for the research community. By leveraging this open-access resource, we aim to advance our understanding of autism and related neurodevelopmental disorders.

References

Aoki, S., Kagitani-Shimono, K., Matsuzaki, J., Hanaie, R., Nakanishi, M., Tominaga, K., Nagai, Y., Mohri, I., and Taniike, M. (2019). Lesser suppression of response to bright visual stimuli and visual abnormality in children with autism spectrum disorder: a magnetoencephalographic study. *Journal of Neurodevelopmental Disorders*, 11.

Ashburner, J. and Friston, K. J. (2005). Unified segmentation. *Neuroimage*, 26(3):839–851.

Attanasio, M., Mazza, M., Le Donne, I., Nigri, A., and Valenti, M. (2024). Salience network in autism: Preliminary results on functional connectivity analysis in resting state. *European Archives of Psychiatry and Clinical Neuroscience*, 275:2479–2492.

Bi, X.-a., Zhao, J., Xu, Q., Sun, Q., and Wang, Z. (2018). Abnormal functional connectivity of resting state network detection based on linear ica analysis in autism spectrum disorder. *Frontiers in Physiology*, 9:475.

Brentani, H., Paula, C. S. d., Bordini, D., Rolim, D., Sato, F., Portolese, J., Pacifico, M. C., and McCracken, J. T. (2013). Autism spectrum disorders: an overview on diagnosis and treatment. *Brazilian Journal of Psychiatry*, 35:S62–S72.

Bullmore, E. and Sporns, O. (2009). Complex brain networks: graph theoretical analysis of structural and functional systems. *Nature reviews neuroscience*, 10(3):186–198.

Canario, E., Chen, D., and Biswal, B. (2021). A review of resting-state fMRI and its use to examine psychiatric disorders. *Psychoradiology*, 1(1):42–53.

Chu, W., Wang, Q., Zhang, L., Gao, Y., and Qian, P. (2022). Multiscale graph representation learning for autism identification with fmri. *Frontiers in Neuroinformatics*, 16:857113.

Di Martino, A. and Mostofsky, S. (2023). Autism brain imaging data exchange (abide).

Duan, Y. M., Zhao, Z., Luo, L., Liu, X., Jiang, T., Tang, B., Liu, S., and Yao, D. (2022). Identifying and predicting autism spectrum disorder based on multi-feature integration of structural mri data. *Frontiers in Human Neuroscience*, 15:765517.

Ebadi, A., Dalboni da Rocha, J. L., Nagaraju, D. B., Tovar-Moll, F., Bramati, I., Coutinho, G., Sitaram, R., and Rashidi, P. (2017). Ensemble classification of alzheimer's disease and mild cognitive impairment based on complex graph measures from diffusion tensor images. *Frontiers in neuroscience*, 11:56.

Ecker, C., Bookheimer, S. Y., and Murphy, D. G. (2015). Neuroimaging in autism spectrum disorder: brain structure and function across the lifespan. *The Lancet Neurology*, 14(11):1121–1134.

Elumalai, P., Yadav, Y., Williams, N., Saucan, E., Jost, J., and Samal, A. (2022). Graph ricci curvatures reveal atypical functional connectivity in autism spectrum disorder. *Scientific Reports*, 12(1):8295.

Francis, S. M., Camchong, J., Brickman, L., Goelkel-Garcia, L., Mueller, B. A., Tseng, A., Lim, K. O., and Jacob, S. (2019). Hypoconnectivity of insular resting-state networks in adolescents with autism spectrum disorder. *Psychiatry Research: Neuroimaging*, 283:104–112.

Freeman, L. C., Roeder, D., and Mulholland, R. R. (1979). Centrality in social networks: Experimental results. *Social networks*, 2(2):119–141.

Hallmayer, J., Cleveland, S., Torres, A., Phillips, J., Cohen, B., Torigoe, T., Miller, J., Fedele, A., Collins, J., Smith, K., et al. (2011). Genetic heritability and shared environmental factors among twin pairs with autism. *Archives of general psychiatry*, 68(11):1095–1102.

Harlalka, V., Naik, S., Bapi, R. S., Vinod, P., and Roy, D. (2018). Integration and segregation in autism spectrum disorders modulated by age, disease, and interaction: a graph theoretic study of intrinsic functional connectivity. *bioRxiv*, page 278846.

Iswarya, M., Raja, R., Rajchakit, G., Cao, J., Alzabut, J., and Huang, C. (2019). Existence, uniqueness and exponential stability of periodic solution for discrete-time delayed BAM neural networks based on coincidence degree theory and graph theoretic method. *Mathematics*, 7(11):1055.

Itahashi, T., Yamada, T., Watanabe, H., Nakamura, M., Jimbo, D., Shioda, S., Toriizuka, K., Kato, N., and Hashimoto, R. (2014). Altered network topologies and hub organization in adults with autism: a resting-state fmri study. *PloS one*, 9(4):e94115.

Kazeminejad, A. and Sotero, R. C. (2019). Topological properties of resting-state fMRI functional networks improve machine learning-based autism classification. *Frontiers in neuroscience*, 12:1018.

Keown, C. L., Datko, M. C., Chen, C. P., Maximo, J. O., Jahedi, A., and Müller, R.-A. (2017). Network organization is globally atypical in autism: a graph theory study of intrinsic functional connectivity. *Biological Psychiatry: Cognitive Neuroscience and Neuroimaging*, 2(1):66–75.

Lee, Y., Park, B.-y., James, O., Kim, S.-G., and Park, H. (2017). Autism spectrum disorder related functional connectivity changes in the language network in children, adolescents and adults. *Frontiers in Human Neuroscience*, 11:418.

Li, Z., Yang, L., Chen, H., Fang, Y., Zhang, T., Yin, X., Man, J., Yang, X., and Lu, M. (2022). Global, regional and national burden of autism spectrum disorder from 1990 to 2019: results from the global burden of disease study 2019. *Epidemiology and Psychiatric Sciences*, 31:e33.

Ma, L., Yuan, T., Li, W., Guo, L., Zhu, D., Wang, Z., Liu, Z., Xue, K., Wang, Y., Liu, J., Man, W., Ye, Z., Liu, F., and Wang, J. (2022). Dynamic functional connectivity alterations and their associated gene expression pattern in autism spectrum disorders. *Frontiers in Neuroscience*, 15:794151.

Millan, M. J., Goodwin, G. M., Meyer-Lindenberg, A., and Ögren, S. O. (2015). Learning from the past and looking to the future: emerging perspectives for improving the treatment of psychiatric disorders. *European Neuropsychopharmacology*, 25(5):599–656.

Nickl-Jockschat, T., Habel, U., Michel, T., Manning, J., Laird, A., Fox, P., Schneider, F., and Eickhoff, S. (2012). Brain structure anomalies in autism spectrum disorder—a meta-analysis of vbm studies using anatomic likelihood estimation. *Human Brain Mapping*, 33:1479–1498.

Nieto-Castanon, A. and Whitfield-Gabrieli, S. (2021). CONN functional connectivity toolbox (rrid: Scr_009550), version 21.

Odriozola, P., Uddin, L. Q., Lynch, C. J., Kochalka, J., Chen, T., and Menon, V. (2016). Insula response and connectivity during social and non-social attention in children with autism. *Social Cognitive and Affective Neuroscience*, 11(3):433–444.

Poldrack, R. A. (2007). Region of interest analysis for fMRI. *Social cognitive and affective neuroscience*, 2(1):67–70.

Pourmotahari, F., Borumandnia, N., Ebrahimzadeh, A., and Habibi, H. R. (2024). Secondary analysis: Graph analysis of brain connectivity network in autism spectrum disorder. *J Res Med Sci*, 29(1):2.

Qian, S., Yang, Q., Cai, C., Dong, J., and Cai, S. (2024). Spatial-temporal characteristics of brain activity in autism spectrum disorder based on hidden markov model and dynamic graph theory: A resting-state fmri study. *Brain Sciences*, 14(5):507.

Retico, A., Gori, I., Giuliano, A., Muratori, F., and Calderoni, S. (2016). One-class support vector machines identify the language and default mode regions as common patterns of structural alterations in young children with autism spectrum disorders. *Frontiers in Neuroscience*, 10:306.

Sadeghi, M., Khosrowabadi, R., Bakouie, F., Mahdavi, H., Eslahchi, C., and Pouretemad, H. (2017). Screening of autism based on task-free fmri using graph theoretical approach. *Physica A: Statistical Mechanics and its Applications*, 473:566–582.

Sadeghian, S., Li, X., and Seltzer, M. (2025). Hyperbrain: Anomaly detection for temporal hypergraph brain networks. In Bathula, D. R., Benet Nirmala, A., Dvornek, N. C., Govindarajan, S. T., Habes, M., Kumar, V., Nebli, A., Wolfers, T., and Xiao, Y., editors, *Machine Learning in Clinical Neuroimaging*, pages 35–45, Cham. Springer Nature Switzerland.

Sewani, H. and Kashef, R. F. (2020). An autoencoder-based deep learning classifier for efficient diagnosis of autism. *Children*, 7(10):182.

Shi, Y., Zhang, L., Wang, Y., Zhan, L., Liu, Y., and Zhou, T. (2020). An fmri feature selection method based on a minimum spanning tree for identifying patients with autism. *Frontiers in Neuroinformatics*, 14:1–10.

Soussia, M. and Rekik, I. (2018). Unsupervised manifold learning using high-order morphological brain networks derived from t1-w mri for autism diagnosis. *Frontiers in neuroinformatics*, 12:70.

Toyomaki, A. and Murohashi, H. (2013). Salience network dysfunction hypothesis in autism spectrum disorders. *Japanese Psychological Research*, 55(2):175–185.

Vankara, K., Muni, D., Rao, K., and Kumar, R. (2024). A novel autism spectrum disorder detection using multi-label graph convolutional network with label-attentive neighborhood convolution. *Computers in Biology and Medicine*, 173:108095.

Wang, M., Ma, Z., Wang, Y., Liu, J., and Guo, J. (2023). A multi-view convolutional neural network method combining attention mechanism for diagnosing autism spectrum disorder. *PLOS ONE*, 18(12):e0295621.

Wang, X. and Ding, J. (2025). Innovative biomarker exploration in autism spectrum disorder: Combining graph neural networks and permutation testing. *NeuroImage: Reports*, 5(2):100249.

Xu, S., Li, M., Yang, C., Fang, X., Ye, M., Wei, L., Liu, J., Li, B., Gan, Y.-g., Yang, B., Huang, W., Li, P., Meng, X., Wu, Y., and Jiang, G. (2019). Altered functional connectivity in children with low-function autism spectrum disorders. *Frontiers in Neuroscience*, 13:806.

Yang, L., Chen, X., Li, X., Shen, Y. Q., Wang, H., Liu, J. R., Mei, T., Ji, Z., Guo, Y., Wang, F., Xu, L., Tang, X., Ma, Z., Wang, L., Liu, J., Cao, Q., and Yan, C. (2018). Altered developmental trajectories in intrinsic function between default, salience, and executive networks in high-functioning autism. *bioRxiv*.

Zamani, J., Sadr, A., and Javadi, A.-H. (2022). Classification of early-MCI patients from healthy controls using evolutionary optimization of graph measures of resting-state fMRI, for the Alzheimer's disease neuroimaging initiative. *Plos one*, 17(6):e0267608.

Zeidan, J., Fombonne, E., Scorah, J., Ibrahim, A., Durkin, M. S., Saxena, S., Yusuf, A., Shih, A., and Elsabbagh, M. (2022). Global prevalence of autism: A systematic review update. *Autism research*, 15(5):778–790.